JACS
JOURNAL OF THE AMERICAN CHEMICAL SOCIETY
Communication
pubs.acs.org/JACS

Atomic-Scale Evolution of a Growing Core−Shell Nanoparticle

Shai Mangel,[†] Eran Aronovitch,[†] Andrey N. Enyashin,[‡] Lothar Houben,[§] and Maya Bar-Sadan*,[†]

[†]Department of Chemistry, Ben-Gurion University of the Negev, Beer-Sheva 84105, Israel

[‡]Institute of Solid State Chemistry UB RAS, Ekaterinburg 620219, Russian Federation

[§]Peter Grünberg Institut 5 and Ernst Ruska-Centre for Microscopy and Spectroscopy with Electrons, Forschungszentrum Jülich GmbH, 52425 Jülich, Germany

Supporting Information

ABSTRACT: Understanding the atomic-scale growth at solid/solution interfaces is an emerging frontier in molecular and materials chemistry. This is particularly challenging when studying chemistry occurring on the surfaces of nanoparticles in solution. Here, we provide atomic-scale resolution of growth, in a statistical approach, at the surfaces of inorganic nanoparticles by state-of-the-art aberration-corrected transmission electron microscopy (TEM) and focal series reconstruction. Using well-known CdSe nanoparticles, we unfold new information that, for the first time, allows following growth directly, and the subsequent formation of CdS shells. We correlate synthetic procedures with resulting atomic structure by revealing the distribution of lattice disorder (such as stacking faults) within the CdSe core particles. With additional sequential synthetic steps, an ongoing transformation of the entire structure occurs, such that annealing takes place and stacking faults are eliminated from the core. The general strategy introduced here can now be used to provide equally revealing atomic-scale information concerning the structural evolution of inorganic nanostructures.

Unfolding the intricate nature of the interactions, reactions and processes at the interface between a growing solid surface and a surrounding solution at an atomic resolution is a fundamental field in science. It is even more challenging when the solid surface is the interface of a nanoparticle in solution due to size and curvature. However, understanding such processes and the means of controlling them is a prerequisite for deliberately placing single atoms into specific structures. Otherwise, forming function-oriented and applications-driven tailor-made nanoparticles remains beyond our reach.

One example of this problem is the colloidal synthesis of core−shell semiconductor nanoparticles, a delicate procedure wherein accurate control over the size and morphology of the nanoparticles is generally produced by kinetic processes. In the past two decades, semiconducting core−shell nanoparticles have been some of the most extensively studied systems in nanoscience.[1] Nevertheless, producing high-quality particles that are chemically and optically stable is still a long-standing problem.[2] Specifically, a direct correlation is currently missing between the synthetic procedures and the atomic rearrangement that is associated with degradation and instability of the optical properties (such as blinking).[3] One of the main concerns in the field is the control over the uniformity of the crystallographic phase, i.e., maintaining the lattice arrangement throughout the growth without the occurrence of defects, such as stacking faults (SF). The CdSe@CdS core−shell system has been used as a model system to study such problems, and effort has been devoted to exclusively grow either the hexagonal wurtzite or the cubic zinc blende phases of these particles.

The main challenge in tackling such issues is to collect and analyze large experimental data sets for statistical purposes, while providing the characteristics of each nanoparticle at the atomic scale. However, today, most characterization procedures used to investigate the morphology and properties of nanoparticles are indirect and average the properties of ensembles of a number of particles, thus hindering our understanding of fundamental aspects of the colloidal synthesis. Reports on the optical properties of single particles are already available,[4] but they do not provide correlations to the atomic structure. Indeed, lower resolution information[5] has demonstrated that the analysis of ensembles masks the distinct spectroscopic behavior of nanoparticle subpopulations, highlighting the importance of correlating morphology and performance.

Although atomic-resolution microscopy may serve as an appropriate characterization tool, it has thus far mainly provided analyses of only a few particles per sample,[6] thus limiting the discussion to only a few particular cases. Importantly, the main reason for this limitation is that collecting the relevant data requires immense efforts due to radiation damage and a general lack of stability under the electron beam of the transmission electron microscope (TEM). Here, we thus monitored the growth evolution of CdSe nanoparticles and the formation of the CdS shell surrounding each particle using aberration-corrected TEM. The high-resolution imaging allowed resolving individual Cd and Se columns. Knowing that the growth direction of the particle is from the nucleus side to the more reactive Se-terminated facet,[6a] we were able to monitor the addition of atomic planes in time and correlate it with the macroscopic synthetic procedure, thus fully explaining the growth process and stacking fault distribution according to simple models.

CdSe cores were synthesized, according to the standard procedure described by Amirav et al.,[4a] using CdO, hexadecyl-

Received: June 28, 2014
Published: August 26, 2014

dx.doi.org/10.1021/ja506323s | J. Am. Chem. Soc. 2014, 136, 12564−12567

amine (HDA) and octadecyl phosphonic acid (ODPA) as precursors (see Supporting Information (SI) for a detailed description). The analysis of large data sets was facilitated by a new-generation aberration-corrected TEM, which corrects both chromatic and spherical aberrations and allows superior resolution in low operating voltages (80 kV) to significantly reduce radiation damage to the samples. Initially, common characterization methods (i.e., optical absorption, photoluminescence, and powder X-ray diffraction [XRD]) were applied to compare our data with the vast data available in the literature. Thereafter, the additional information acquired by high-resolution TEM was used to provide a more complete understanding of the synthetic process.

The ensemble optical absorption and photoluminescence properties showed the characteristic features of CdSe nanoparticles (Figure 1a,b). However, these techniques cannot

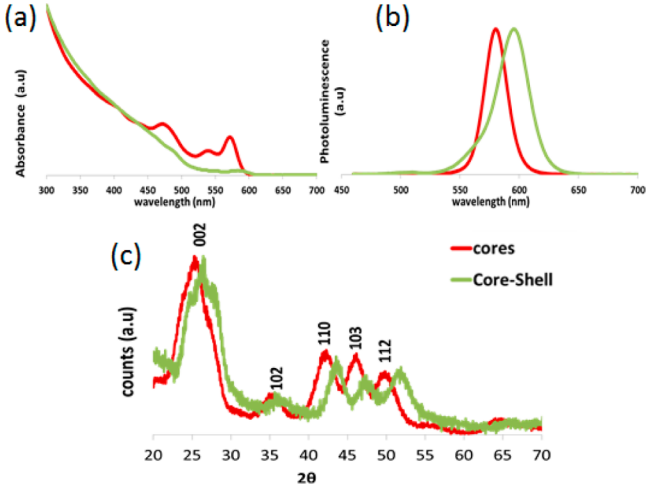

Figure 1. Absorbance spectra (a), photoluminescence (PL) spectra (b), and XRD patterns of the CdSe cores and the core−shell CdSe@CdS particles (c). CdSe cores in red, CdSe@CdS in green. PL excitation wavelength in (b): 440 nm. The X-ray count rates in (c) were normalized to the overall signal.

answer questions about the distribution of stacking faults during the growth process. In the size regime of less than 4 nm, the optical absorbance of the hexagonal wurtzite and the cubic zinc blende phases is similar in terms of the correlation between the first absorbance peak and the size of the particle.[7] Theoretically, and as shown previously in some experimental work,[3b,7b] the gap between the first ($1S_{3/2}1S_e$) and second ($2S_{3/2}1S_e$) energy transitions is large enough to identify the zinc blende phase, whereas a short distance between these two peaks points to a wurtzite phase. However, there is no theoretical treatment for a mixed state with stacking faults. Therefore, the first exciton absorption peak in the present work was used only to calculate the particle size, resulting in an estimation of 3.5 nm. The photoluminescence shows a sharp, narrow peak at 580 nm, with a full-width half-maximum (fwhm) of 22 nm, indicating a narrow size distribution.

XRD patterns of the CdSe particles showed mainly the wurtzite phase, as was expected given the synthetic protocol used (Figure 1c). Lacking information on individual particles, the seminal paper by Murray et al.[8] that was published two decades ago used the Debye scattering model and postulated what is today the common approach for the characterization of CdSe nanoparticles by powder XRD diffraction. The number of stacking faults is estimated from the XRD patterns by using the ratio of the (103) peak of the wurtzite structure relative to its two neighbors: the (110) and (112) peaks.[8,9] In pure wurtzite CdSe, this peak is higher than the (112) peak and similar to the (110) peak. According to the simulations by Murray et al.,[8] the height of the (103) peak is highly sensitive to the occurrence of even a single stacking fault in the structure, as well as to the location of the fault within the particle.

Herein, the core particles exhibited the required benchmark fingerprint of high-quality CdSe nanoparticles: a well-pronounced (103) peak. The lattice parameters extracted from the XRD patterns showed a contraction in the *a* lattice parameter (0.87%) and a small expansion in the *c* parameter (0.21%), compared with the wurtzite parameters of bulk CdSe. This result is in accordance with values reported in the literature for crystals close to 4 nm in size.[10]

Taken together, the properties of the ensemble gave only partial information on the occurrence and distribution of stacking faults, since optical characterization is not sufficiently sensitive for a mixed-state situation, and XRD can be interpreted only indirectly using a model. Hence, to attain the required information regarding the stacking faults distribution pattern directly, images of the nanoparticles were taken on a FEI Ultimate 60-300 ("PICO") TEM at 80 kV, with both spherical and chromatic aberration correction.[11] A focal series of images was used to reconstruct the exit-plane wavefunction[12] in tandem with optimized phase contrast imaging (see SI for a detailed description of TEM acquisition and image processing). Next, the location of the heavier Cd columns was identified according to their higher intensity on the image compared with the S columns (Figure 2a). Large data sets of 15−25 CdSe and CdSe@CdS particles were reconstructed to provide a quantitative statistical analysis.

The particles were divided into four along the hexagonal *c* axis, with the first quarter at the Cd-terminated side and the fourth quarter at the Se-terminated side. The histograms describing the occurrence of stacking faults within these four quarters are presented in Figure 3, where the overall size of the CdSe core is shown inside the gray dashed frame.

This analysis shows a low average of 0.80 stacking faults per core particle; however, the location of the stacking faults along the particle differs significantly from that in the model presented by Murray et al.[8] Specifically, instead of a single fault in the center of the particle, as predicted by the model, we show that most stacking faults are concentrated in the first quarter (closer to the Cd edge), somewhat less stacking faults are concentrated in the fourth quarter (closer to the Se edge), and the lowest density of stacking faults is found on the two central quarters of the particle (Figure 3). This distribution of stacking faults is in accordance with the well-accepted growth kinetics,[3b] where the *c* direction is the growth front of the reaction such that the faster growth occurs on the Se-terminated facet. At the reaction front, the ligands are less strongly attached, allowing the building blocks in the solution access to the interface of the particle. The faster addition of atoms to one facet of the particle creates directional growth and a final oval shape. Growth also proceeds at the Cd-terminated facet, albeit at a slightly slower rate.[3b]

The highest concentration of faults at the Cd-terminated facet may be associated with the retention of early disorder, already created in the nucleation step, as the nucleus of the nanoparticle may have a disordered structure (i.e., neither wurtzite nor zinc blende symmetry[7b]) or it may comprise a

dx.doi.org/10.1021/ja506323s | J. Am. Chem. Soc. 2014, 136, 12564−12567

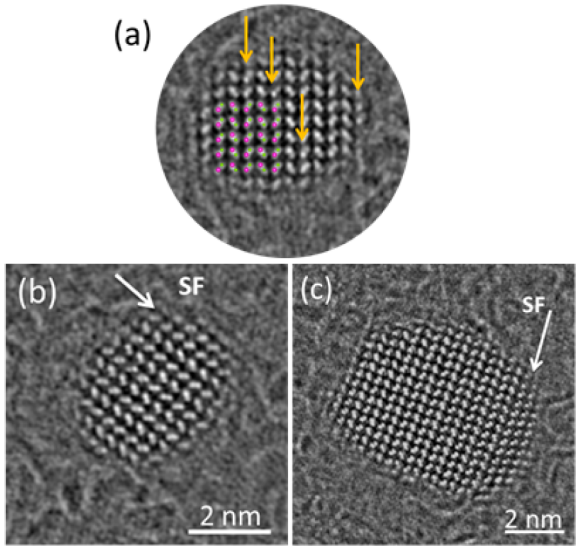

Figure 2. Phase image of exit-plane wavefunctions reconstructed from a through-focus series. (a) A CdSe nanoparticle. Arrows point to the higher intensity columns of the Cd. An atomic model of hexagonal wurtzite CdSe is overlaid on the image, showing the Cd in purple and the Se in green. (b) A CdSe nanoparticle. Arrow points to a stacking fault (SF). (c) A CdSe@CdS core–shell particle. Arrow points to a fault: a transformation from a wurtzite structure (left side of image) to a zinc blende structure (right side of image). All wavefunctions were Fourier filtered to eliminate the background pattern of the periodic hexagonal graphene support film.

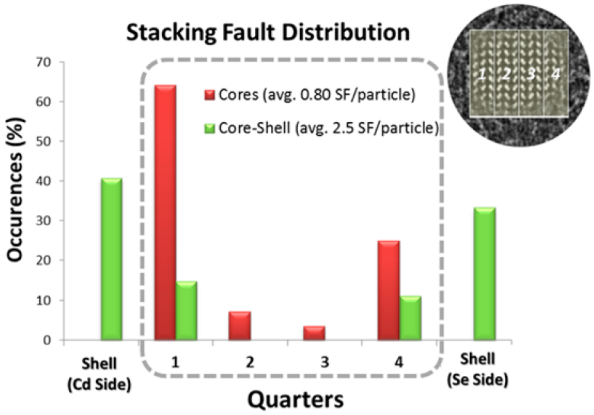

Figure 3. Histogram describing the distribution of stacking faults of CdSe particles in the ⟨001⟩ growth front direction. The particle is divided to quarters, with the first quarter beginning with the Cd layer and the fourth quarter ending with the Se layer (see inset for schematic representation). Red columns indicate the CdSe cores, and green columns indicate the CdSe@CdS particles that were synthesized with the sample of cores. Large data sets of 15–25 CdSe and CdSe@CdS particles were reconstructed to provide a quantitative statistical analysis.

complete zinc blende phase.[1] Other findings suggest that the slower growth rate points to specific kinetics that also produce more faults at the Cd growth front.[3b]

Because the growth advances mainly in one direction, i.e., from the Cd edge to the Se edge, our analysis also reveals the formation of the stacking faults in time. The growth phase occurs as the temperature rises from 330 °C (after injection of the reactants) to 360 °C, which is more suitable for the growth of the wurtzite phase. Therefore, the reduction in fault density observed as the reaction progresses is attributed to the gradual change in temperature. Once the reaction is halted by removing the heating mantle, the growth does not stop immediately, and the last atomic planes are probably deposited with greater disorder, leaving defects in the last quarter.

In a subsequent step, the CdS shell was grown on the same CdSe core sample according to a modified procedure based on a thermal cycling protocol.[11,13] The final size of the particles was about 6.8 nm, and they exhibited only a slightly oval structure with an aspect ratio of 1.20. The size difference between the core and shell points to a shell thickness of 4–5 monolayers of CdS.

Absorption and photoluminescence spectra show the formation of a fully covering CdS shell (see the green curves in Figure 1a,b), and energy-filtered TEM (EFTEM) images show an almost concentric core–shell structure (SI). Both the photoluminescence peak and the absorbance features shift to lower energy (red shift), by about 15 nm with respect to the original CdSe peaks, due to the broad delocalization of the excited electrons to the shell area[14] and the fwhm broadened to 31 nm. The XRD patterns (see the green curve in Figure 1c) retain a single phase in hexagonal symmetry, but the entire pattern is shifted to higher angles, demonstrating a transition from CdSe bulk lattice parameters to the smaller values of CdS.[8] The final lattice parameters show an intermediate value between the CdSe and CdS lattice parameters, with a slight expansion from the bulk values of CdS and a significant contraction from the CdSe values. The height of the (103) peak of the core–shell particles relative to the (110) and (112) peaks is only slightly attenuated compared with that of the CdSe core sample.

Quantitative TEM analysis of the core–shell particles, performed in the same manner as that for the CdSe particles, revealed a much higher number of stacking faults, namely, an average of 2.5 stacking faults per particle, which was unexpected considering the pronounced (103) reflection in the XRD pattern. The shell dimensions were calculated to comprise 4–5 CdS monolayers, enabling the marking of the CdSe/CdS interface. The CdSe core of the particles was again divided into four quarters, allowing comparison with the stacking fault distribution of the original cores. The central core region, which previously had only a few stacking faults, was now completely defect free. We ascribe this finding to the additional annealing processes provided by the subsequent deposition of the shell layers, and specifically to the additional time at 250 °C following the S precursor injections. In contrast, the shell regions and their immediate environment, i.e., the first and fourth quarters of the CdSe core, were now rich in stacking faults. The denser concentration of faults was seen at the shell regions, probably due to the remaining disorder of the exterior atomic shells following the core synthesis.

While the cores contained mainly wurtzite crystals, with an occasional zinc blende plane usually at the very edge of the particle, the core–shell particles typically contained a phase transformation from wurtzite to zinc blende at the interface between the core and shell. The CdS shell has smaller lattice dimensions than the CdSe, which exerts strain on the CdSe core. Density functional theory (DFT) calculations of infinite planes show very little influence of the strain, induced by the 4% mismatch in lattice parameters between CdSe and CdS, on the energy of the interfaces. Thus, the core–shell geometry is probably the main factor in the formation of these phase transitions.

dx.doi.org/10.1021/ja506323s | J. Am. Chem. Soc. 2014, 136, 12564–12567

With the new findings, it is possible to complete the details of the overall growth process; the nucleation step produces a disordered structure, part of which is retained as the growth progresses. During this process, the temperature rises and conditions become more suitable for the formation of the wurtzite phase, resulting in directional growth, and the particle elongates. At this stage, the occurrence of stacking faults is less likely. When the reaction is halted, the disorder of the very last atomic planes at the growth front is frozen. Upon resumption of the growth to produce the shell, the conditions are more compatible with the formation of CdS in the isotropic zinc blende phase, due to the temperature regime and the accumulated strain. Stacking faults are produced at the interface between the core and the shell, and the newly grown shell acquires the zinc blende phase. During this process, the temperature is high enough to allow annealing of the core so that stacking faults are eliminated toward the interface with the shell.

This picture of the growth process was supported by a control experiment, confirming that pure CdS particles produced under these experimental conditions acquire the zinc blende phase, in accordance with the shell structure. Furthermore, the loss of directional growth due to the transformation into the isotropic zinc blende phase was manifested in the decrease of the aspect ratio from 1.50 for the cores to 1.20 for the core−shell structures. Moreover, these phase transformations are typical[15] even for bulk CdSe under pressure (around 2.5 GPa), producing a lamellar structure of 3−5 zinc blende layers and a zinc blende-to-wurtzite ratio of 20:80, similar to our present findings.

In summary, our results show that, at least for the growth process of the model system investigated here, solid/solution interfaces can be monitored at the atomic level using aberration-corrected TEM and focal series reconstruction that assigns polarity to CdSe and CdSe@CdS core−shell particles. Moreover, we also demonstrated that the formation of stacking faults can be successfully correlated with the progression of the reaction. The complete picture, as revealed by the TEM analysis, is significantly different from the information provided by ensemble analysis and indirect methods alone. Specifically, the atomic rearrangement of the particles (i.e., stacking faults, their distribution pattern along the growth axis, and phase transformations) was not detected by the common characterization methods of XRD, optical absorption and photoluminescence, as opposed to the detailed information provided by the TEM analysis. We conclude that high-resolution electron microscopy and acquisition schemes such as focal series reconstruction can serve as a routine tool using a statistical approach for understanding growth kinetics and can be used to characterize the atomic rearrangements in a hybrid particle synthesis that requires multiple steps. This strategy can be applied to other hybrid structures, where kinetic procedures determine the nature and properties of interfaces, providing a more complete atomic-scale picture of unidirectional epitaxial growth.

■ ASSOCIATED CONTENT

Supporting Information

An extended Materials and Methods section, including details of the synthesis, calculations and image analysis. This material is available free of charge via the Internet at http://pubs.acs.org.

■ AUTHOR INFORMATION

Corresponding Author

barsadan@bgu.ac.il

Notes

The authors declare no competing financial interest.

■ ACKNOWLEDGMENTS

This research project was supported by The Israeli Centers of Research Excellence (I-CORE) program, (Center No. 152/11), ISF grant 475/12, the Adelis Fund, and the European Union Seventh Framework Programme, under Grant Agreement 312483-ESTEEM2 (Integrated Infrastructure Initiative-I3). M.B.-S. appreciates support from Dr. Vladimir Ezersky, Dr. Yael Levi-Kalisman, and Dr. Dmitri Mogilyanski of the Ilse Katz Institute for Nanoscale Science Technology, and of Dr. Lisa Shandalov, Dr. Sudheendran Mavila and Mr. Yakov Ginzburg, of the Department of Chemistry. M.B.-S. also thanks Prof. Taleb Mokari and Prof. Ira Weinstock (Ben-Gurion University of the Negev) for brainstorming and constructive criticism.

■ REFERENCES

(1) Yin, Y.; Alivisatos, A. P. *Nature* **2005**, *437*, 664.

(2) Chen, O.; Zhao, J.; Chauhan, V. P.; Cui, J.; Wong, C.; Harris, D. K.; Wei, H.; Han, H.-S.; Fukumura, D.; Jain, R. K.; Bawendi, M. G. *Nat. Mater.* **2013**, *12*, 445.

(3) (a) Gao, Y.; Peng, X. *J. Am. Chem. Soc.* **2014**, *136*, 6724. (b) Hughes, S. M.; Alivisatos, A. P. *Nano Lett.* **2012**, *12*, 106.

(4) (a) Amirav, L.; Alivisatos, A. P. *J. Phys. Chem. Lett.* **2010**, *1*, 1051. (b) Talapin, D. V.; Koeppe, R.; Götzinger, S.; Kornowski, A.; Lupton, J. M.; Rogach, A. L.; Benson, O.; Feldmann, J.; Weller, H. *Nano Lett.* **2003**, *3*, 1677.

(5) Borys, N. J.; Walter, M. J.; Huang, J.; Talapin, D. V.; Lupton, J. M. *Science* **2010**, *330*, 1371.

(6) (a) Rosenthal, S. J.; McBride, J.; Pennycook, S. J.; Feldman, L. C. *Surf. Sci. Rep.* **2007**, *62*, 111. (b) McBride, J.; Treadway, J.; Feldman, L. C.; Pennycook, S. J.; Rosenthal, S. J. *Nano Lett.* **2006**, *6*, 1496. (c) McBride, J. R.; Kippeny, T. C.; Pennycook, S. J.; Rosenthal, S. J. *Nano Lett.* **2004**, *4*, 1279. (d) Bertoni, G.; Grillo, V.; Brescia, R.; Ke, X.; Bals, S.; Catellani, A.; Li, H.; Manna, L. *ACS Nano* **2012**, *6*, 6453.

(7) (a) Karel čapek, R.; Moreels, I.; Lambert, K.; De Muynck, D.; Zhao, Q.; Van Tomme, A.; Vanhaecke, F.; Hens, Z. *J. Phys. Chem. C* **2010**, *114*, 6371. (b) Harrell, S. M.; McBride, J. R.; Rosenthal, S. J. *Chem. Mater.* **2013**, *25*, 1199.

(8) Murray, C. B.; Norris, D. J.; Bawendi, M. G. *J. Am. Chem. Soc.* **1993**, *115*, 8706.

(9) Guinier, A. *X-ray Diffraction in Crystals, Imperfect Crystals, and Amorphous Bodies*; W. H. Freeman: San Francisco, 1963.

(10) Masadeh, A. S.; Božin, E. S.; Farrow, C. L.; Paglia, G.; Juhas, P.; Billinge, S. J. L.; Karkamkar, A.; Kanatzidis, M. G. *Phys. Rev. B* **2007**, *76*, 115413.

(11) Haider, M.; Hartel, P.; Mueller, H.; Uhlemann, S.; Zach, J. *Microsc. Microanal.* **2010**, *16*, 393.

(12) Thust, A.; Coene, W. M. J.; Op de Beeck, M.; Van Dyck, D. *Ultramicroscopy* **1996**, *64*, 211.

(13) Blackman, B.; Battaglia, D. M.; Mishima, T. D.; Johnson, M. B.; Peng, X. *Chem. Mater.* **2007**, *19*, 3815.

(14) (a) Li, J. J.; Wang, Y. A.; Guo, W.; Keay, J. C.; Mishima, T. D.; Johnson, M. B.; Peng, X. *J. Am. Chem. Soc.* **2003**, *125*, 12567. (b) Xie, R.; Kolb, U.; Li, J.; Basche, T.; Mews, A. *J. Am. Chem. Soc.* **2005**, *127*, 7480.

(15) Leoni, S.; Ramlau, R.; Meier, K.; Schmidt, M.; Schwarz, U. *Proc. Natl. Acad. Sci. U.S.A.* **2008**, *105*, 19612.